New Phytologist

Research

Deviation from symmetrically self-similar branching in trees predicts altered hydraulics, mechanics, light interception and metabolic scaling

Duncan D. Smith[1], John S. Sperry[1], Brian J. Enquist[2], Van M. Savage[3], Katherine A. McCulloh[4,5] and Lisa P. Bentley[2]

[1]Department of Biology, University of Utah, Salt Lake City, UT 84112, USA; [2]Department of Ecology and Evolutionary Biology, University of Arizona, Tucson, AZ 85721 USA; [3]Department of Biomathematics, University of California, Los Angeles, CA 90095, USA; [4]Department of Forest Ecosystems and Society, Oregon State University, Corvallis, OR 97331, USA; [5]Present address: Department of Botany, University of Wisconsin-Madison, Madison, WI 53706, USA

Author for correspondence:
Duncan D. Smith
Tel: +1 801 585 0381
Email: duncan.smith@utah.edu

Received: *1 May 2013*
Accepted: *8 August 2013*

New Phytologist (2013)
doi: 10.1111/nph.12487

Key words: branching symmetry, Euler buckling, hydraulic architecture, light interception, metabolic scaling theory, plant allometry, West Brown and Enquist.

Summary

- The West, Brown, Enquist (WBE) model derives symmetrically self-similar branching to predict metabolic scaling from hydraulic conductance, K, (a metabolism proxy) and tree mass (or volume, V). The original prediction was $K \propto V^{0.75}$. We ask whether trees differ from WBE symmetry and if it matters for plant function and scaling. We measure tree branching and model how architecture influences K, V, mechanical stability, light interception and metabolic scaling.
- We quantified branching architecture by measuring the path fraction, P_f: mean/maximum trunk-to-twig pathlength. WBE symmetry produces the maximum, $P_f = 1.0$. We explored tree morphospace using a probability-based numerical model constrained only by biomechanical principles.
- Real tree P_f ranged from 0.930 (nearly symmetric) to 0.357 (very asymmetric). At each modeled tree size, a reduction in P_f led to: increased K; decreased V; increased mechanical stability; and decreased light absorption. When P_f was ontogenetically constant, strong asymmetry only slightly steepened metabolic scaling. The P_f ontogeny of real trees, however, was 'U' shaped, resulting in size-dependent metabolic scaling that exceeded 0.75 in small trees before falling below 0.65.
- Architectural diversity appears to matter considerably for whole-tree hydraulics, mechanics, photosynthesis and potentially metabolic scaling. Optimal architectures likely exist that maximize carbon gain per structural investment.

Introduction

A large and growing body of research has focused on the coordination of hydraulic transport with the metabolism of photosynthesis and growth. While empirical research on this subject is quite extensive (e.g. Brodribb, 2009), a prominent component is metabolic scaling theory (MST) which stems from the original development by West, Brown & Enquist (WBE) (1997, 1999). The theory, as it applies to plants, centers on the premise that water transport is a co-limiting factor for photosynthesis. Because water transport is a largely physical process dependent in part upon transport network structure, its scaling can be predicted from relatively simple allometric models, leading to scaling predictions for all dependent metabolic processes.

The WBE model is fairly simple in its design. Plant branching structure is divided into external and internal components. The external structure follows symmetrical and self-similar branching (see Fig. 1a, rightmost tree) which allows the structure to be easily scaled. The external structure also conforms to biomechanical principles of area preservation and safety from gravitational buckling. The internal branching structure is the network of xylem conduits within the branches. The number and dimensions of xylem conduits are linked by simple rules to the external branch network (Savage *et al.*, 2010; Sperry *et al.*, 2012).

Central to MST are relationships described by power functions of the form $y = ax^b$ where a is a scaling multiplier and b is a scaling exponent. Oftentimes, the focus is on the proportionality, $y \propto x^b$. The WBE model's prominent achievement is the analytical prediction in agreement with at least some empirical observations (Niklas & Enquist, 2001) that metabolic rate (B) scales with mass (M) to the 3/4 power (i.e. $B \propto M^{3/4}$; symbol definitions repeated in Table 1). This scaling prediction may be broken into two separate components that individually relate mass and water use to the easily measured dimension of trunk diameter, D_T.

The stem mass (and volume, V) is assumed to scale with $D_T^{1/c}$. This 'volume exponent', c, is predicted to converge on 3/8, which is supported by theoretical and empirical considerations (McMahon & Kronauer, 1976; von Allmen *et al.*, 2012). The rate of water use, Q, is assumed to scale with D_T^q. The model predicts Q from whole-tree hydraulic conductance, K, which is

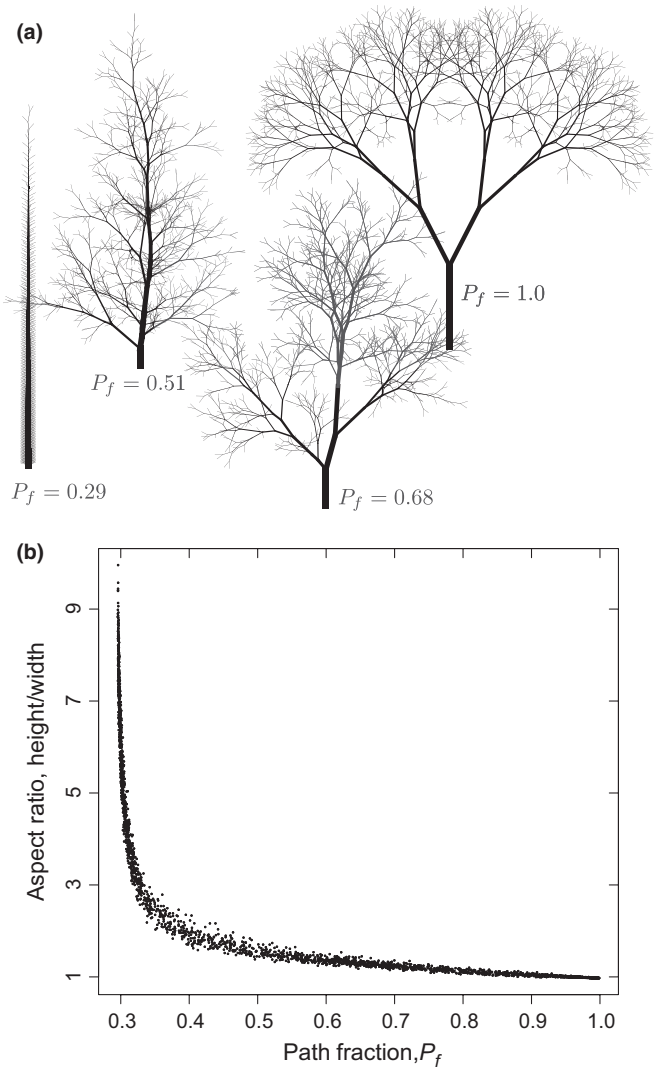

Fig. 1 Tree shape in relation to tree path fraction. Simulations are for trees of the same basal diameter, height, and twig number (1024). Furcation was set to $f^* = 2$ as required when specifying branch angles. (a) The rightmost tree ($P_f = 1$) is the WBE structure with perfect symmetry at each junction. The leftmost tree is the 'fishbone' structure which represents the minimum P_f. The two intermediate trees were generated by the model. (b) The aspect ratio quantifies whole tree shape where an aspect ratio of one may be thought of as a sphere (or hemisphere) while larger values indicate a narrower crown.

Table 1. Symbol definitions and modifiers from the main text in order of appearance

Basic symbols and definitions		Input
B	metabolic rate	
M	mass	
D	stem diameter	
V	total stem volume	
c	'volume exponent' in $M \propto V \propto D_T^{1/c}$	
Q	whole-tree sapflow rate	
K	whole-tree hydraulic conductance	
q	'hydraulic exponent' in $B \propto K \propto D_T^q$	
cq	'metabolic exponent' in $B \propto K \propto V^{cq}$	
P_f	path fraction = mean $L_\uparrow$ / maximum $L_\uparrow$	
$L_\uparrow$	pathlength from trunk base to twig tip	
f	branching junction furcation number	2 to 4
R	rank = number of supported twigs	
A	minimum possible R for a given daughter in a given junction	
Z	maximum possible R for a given daughter in a given junction	
P_{R_d}	probability of choosing a given daughter rank	
u	exponent used to shift P_{R_d} towards choosing A or Z	−5 to 5
$L_\uparrow^*$	maximum pathlength from branch base to twig tip	
a	$L_\uparrow^*$ scaling multiplier ($m^{1/3}$)	26.99
L_{crit}	theoretical $L_\uparrow$ at which tree of given D_T should buckle	
b	L_{crit} scaling multiplier ($m^{1/3}$)	107.94
s	eventual safety factor from buckling	4
l_o	virtual length: distance beyond twig tip to theoretical origin (m)	0.34
l	stem segment length between junctions	
n	scaling exponent for how diameter of main stem varies with height	
m	scaling exponent for how supported mass varies with height	
c_v	first positive root of Bessel function with input, v	
PAR_{abs}	total absorbed photosynthetically active radiation (μmol s^{-1})	
V_f	volume fraction = actual stem volume / volume of a column of equivalent height and basal diameter	
Subscript modifiers		
T	trunk	
m	mother	
d	daughter	
t	twig	
Superscript modifier		
*	maximum	

calculated from internal vascular allometry. If the flow-induced pressure drop from soil to leaf is size invariant, then $K \propto Q$. Because water loss and CO_2 uptake utilize the same stomatal pathway, carbon assimilation should have a direct relationship to Q. If a constant fraction of photosynthate goes towards growth (a proxy for B) the result is $B \propto Q \propto K \propto D_T^q$. The product of the 'hydraulic exponent', q, and c gives the 'metabolic exponent', cq: $B \propto Q \propto K \propto M^{cq}$. The WBE derivation of $cq = 0.75$ arises from the prediction that q converges on 2 for infinitely large trees. Thus, $c = 3/8$, $q = 2$ and $cq = 0.75$. Smaller values of q (0.68–1.91) and, hence, cq (0.25–0.70) are predicted for finite trees (Savage *et al.*, 2010; Sperry *et al.*, 2012).

Since its creation, revisions have been made to the WBE model, which have dealt with altering the branching structure within the confines of perfect symmetry (Price *et al.*, 2007) and making the internal anatomy more realistic. The anatomical modifications have included more accurate scaling of xylem conduit number (Savage *et al.*, 2010) and the addition of leaves, roots and nontransporting tissues (Sperry *et al.*, 2012). These revisions have led to more accurate predictions (Price *et al.*, 2007; von Allmen *et al.*, 2012) but trees were still assumed to follow symmetrically self-similar branching. Real trees show average branching ratios (daughter/mother branch number, diameter and length) that can be similar to the constants predicted by WBE's

symmetric self-similarity (Bentley *et al.*, 2013). However, the distributions are quite broad, indicating a sizable fraction of asymmetric junctions. Even a few asymmetric junctions amongst major branches could significantly alter whole-tree symmetry.

We ask whether the branching architecture of real plants deviates substantially from the WBE structure. We then address the consequences of deviation with a model. We use the WBE model as a reference point and develop a novel numerical simulation method for building trees that represents the full range of tree morphospace from WBE symmetry to maximal asymmetry. Our numerical approach uses a minimum of deterministic branching rules and instead relies on probability distributions to build branch junctions and trees of varying symmetries. Our only major branching assumptions are that trees conform to the well-established patterns of area-preserving branching (Horn, 2000) and network-scale elastic similarity (McMahon & Kronauer, 1976). We use the improved internal anatomy of Sperry *et al.* (2012) but hold xylem parameters constant across simulated trees in order to isolate branching effects. We use the numerical model to investigate how deviations from WBE branching affect whole-tree hydraulic conductance, total stem volume, safety from gravitational buckling, and light interception. The model is also used to predict the influence of branching architecture on the scaling of tree hydraulic conductance (exponent q) and volume (exponent c) with trunk diameter, and hence how hydraulic conductance and its dependent processes scale with mass (exponent cq).

Description

The path fraction index for tree form

We developed the 'path fraction', P_f, to quantify how much a particular branch network deviated from the WBE ideal. The path fraction is based on the pathlengths from twig tip to trunk base. We use the symbol, $L_{\updownarrow}$, for this pathlength where the double arrow indicates that this length spans two extremes, twig tip to trunk base. In a WBE tree, all values of $L_{\updownarrow}$ are the same. In our model, deviating from WBE by removing junction symmetry adds variation to $L_{\updownarrow}$. We define the path fraction as

$$P_f = \frac{\bar{L}_{\updownarrow}}{L^*_{\updownarrow}} \qquad \text{Eqn 1}$$

The bar in $\bar{L}_{\updownarrow}$ refers to the mean $L_{\updownarrow}$ for the tree and the asterisk in $L^*_{\updownarrow}$ (and other symbols that follow) indicates the maximum. The $L^*_{\updownarrow}$ is an approximation of plant height so we will also use this symbol for height. The maximum possible P_f is 1, which occurs when $\bar{L}_{\updownarrow} = L^*_{\updownarrow}$ (e.g. WBE trees; see Fig. 1a, rightmost tree). A high P_f corresponds to a round-shaped, spreading crown while a low P_f corresponds to a narrow crown with limited spread (Fig. 1). The minimum P_f is made by a structure with a central axis with twigs attached alternately. This structure minimizes $\bar{L}_{\updownarrow}$ and we refer to it as the 'fishbone' structure (e.g. Fig. 1a, leftmost tree). We use P_f as the independent branching structure variable against which we plot the functional attributes of tree hydraulic conductance, volume, mechanical stability and light interception.

Empirical path fractions

As a test of how much real plants deviate from the WBE structure, 40 P_f measurements were made of real branch systems. Specimens came from 15 different species and included both whole individuals and branches of open-grown trees and shrubs (species and sources in Table 2 and Supporting Information Notes S1). Species were chosen to represent a wide range of apparent architectures. Branches were obtained by a single cut just distal to a branch junction. Path fractions were obtained in two ways. For some (mostly the entire individuals) each segment between branching points was labeled and its length, diameter

Table 2. Empirical P_f measurements from trees and shrubs

Species	Species Code	Twigs/P_f*	Source†
Acer glabrum	*Ag*	82/0.56	RBC
Acer grandidentatum	Ag	93/0.71, **189/0.64**, **315/0.42**‡	RBC
Acer negundo	An	86/0.50, 130/0.53	RBC
Cornus sericea	Cs	**75/0.79**, 497/0.69	RBC
Elaeagnus angustifolia	Ea	26/0.67	RBC
Fraxinus nigra	Fn	**5/0.92**, **6/0.93**, **10/0.92**, **13/0.84**	CC
Pinus ponderosa	Pp	**10/0.86**‡, **29/0.67**‡, **31/0.85**‡, **33/0.80**‡, **68/0.72**‡	CNF
Populus tremuloides	Pt	81/0.81, **113/0.65**, **118/0.72**	RBC
Quercus ellipsoidalis	Qe	**13/0.83**, **17/0.86**, **34/0.69**, **35/0.78**	CC
Quercus gambelii	Qg	**56/0.62**‡, 71/0.57, 86/0.43, **147/0.63**	RBC
Rhus glabra	Rg	26/0.84	RBC
Rhus trilobata	Rt	174/0.55	RBC
Robinia pseudoacacia	Rp	**25/0.56**, **59/0.64**	CC
Salix exigua	Se	**11/0.88**, **46/0.76**, **48/0.80**	RBC
Ulmus pumila	Up	122/0.56, 227/0.36, 253/0.56, 338/0.55	RBC

*Bold values indicate whole individuals. Branches otherwise.
†RBC, Red Butte Canyon; CNF, Coronado National Forest; CC, Cedar Creek
‡Networks also analyzed by Bentley *et al.* (2013)

and mother segment were recorded. Twig-to-base paths were then reconstructed from these data to get all $L_{\updownarrow}$ values. For the other specimens, $L_{\updownarrow}$ values were measured directly by following stems from base to twig tips using a marked string with 10-cm precision. For this direct method, specimens were measured in spring so the measurements were made to tips that appeared to have been active the previous season.

Direct P_f measurements were time-consuming, limiting the size range to trees with trunk diameters, D_T, < *c.* 5 cm. To estimate the P_f of larger trees to trunk diameters over 1 m, we used the crown area vs trunk diameter dataset of Olson *et al.* (2009) see Fig. S1) from angiosperm trees. From their published data (including all branches and trees in sheltered and salt-sprayed environments), we obtained an OLS regression to predict vertically projected crown areas from D_T. We matched these predictions to 3D modeled trees with the same D_T and within 5% of the same crown area. The P_f from these matching model trees were used to construct a P_f ontogeny.

Tree building model

Branching Our tree building model was written in the R language (R Core Team, 2013) and is available from the senior author upon request. The model begins by sequentially defining junctions, starting with the trunk. At each junction, the mother branch (subscript *m*) splits into a number of daughters (subscript *d*). The number of daughters is *f*, the furcation number. Within each tree, we randomly chose a maximum furcation, f^*, and then at each junction we chose f from 2 to f^*. The f^* was 2, 3 or 4, which covers the range for most botanical trees. Our f selection contrasts with the WBE model which uses a strictly constant f (n in their terminology). We assigned each branch an order or rank, R, equal to the number of twigs it ultimately supports (Katifori & Magnasco, 2012). Therefore, the starting point of each tree, the trunk, has R_m = the total number of twigs on the tree. This ranking system, illustrated in Fig. 2, simplifies tree building because: R is a finite integer; branch ranks change at each junction; and total rank is preserved across junctions. Each combination of mother rank, R_m, and f defines possible daughter ranks, R_d. Each daughter can only take on a certain number of different ranks because the sum of R_d must equal R_m. The first selected daughter rank, $R_{d,1}$, was always the smallest and was restricted to the range, A_1 to Z_1, where $A_1 = 1$ and

$$Z_1 = \lfloor \frac{R_m}{f} \rfloor \qquad \text{Eqn 2}$$

where the floor brackets indicate the integer of the ratio. For subsequent daughter ranks, $R_{d,i}$, where $1 < i \leq f$, the Z_i is given by

$$Z_i = \left\lfloor \left(R_m - \sum_{j=1}^{i-1} R_{d,j} \right) / (f - i + 1) \right\rfloor \qquad \text{Eqn 3}$$

Equation 3 is just a variation on Eqn 2 where the numerator accounts for the fact that there is 'less rank' remaining to divide and the denominator indicates the 'remaining rank' is being divided among fewer undefined daughters. The intermediate values of A_i (if present) are different from the first and final A_i. For $1 < i < f$, the $A_i = R_{d,i-1}$ as no daughter may be smaller than its predecessor. For the final daughter in the furcation, $R_{d,f}$, the $A_f = Z_f$ such that $R_{d,f}$ can only take on a single value that completes the mother rank.

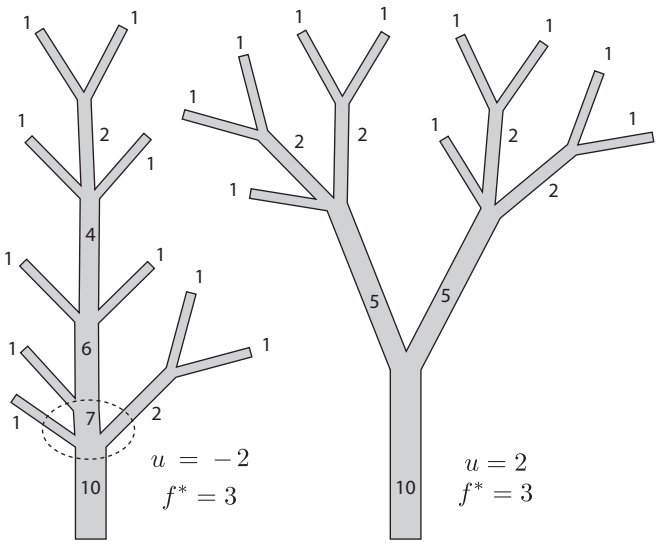

Fig. 2 Two trees with 10 twigs each illustrate several model properties. Numbers at each branch segment indicate the rank, R, where R must balance across each junction. Each rank is chosen at random but the symmetry of each junction and the overall structure is influenced by parameter u. The furcation, f, of each junction is also selected randomly although both trees have the same maximum furcation, f^*. The selection process for the circled junction is detailed in the main text. The trees also show branch diameters (exaggerated) that result from area- and rank-preservation and invariant twigs ($R = 1$). Branch lengths are drawn to scale and reflect the length selection process detailed in the main text.

The choice of R_d in each junction determines the symmetry of that junction. We controlled this choice by using a discrete probability distribution function to select each $R_{d,i}$ at random from its respective A_i to Z_i range. We defined this probability distribution with a power function because changing the exponent, u, allowed us to control the degrees of symmetry or asymmetry. When $u \leq 0$, the probability, P, of any R_d is given by

$$P_{R_d} = R_d^u / \sum_{j=A}^{Z} j^u \qquad \text{Eqn 4}$$

When $u > 0$, a slightly different equation is used,

$$P_{R_d} = (Z - A + R_d)^{-u} / \sum_{j=A}^{Z} (Z - A + j)^{-u} \qquad \text{Eqn 5}$$

For a given $u > 0$, Eqn 5 takes the probabilities from Eqn 4 with $-u$ and mirrors them over the same A to Z range. For example, comparing $u = 2$ to $u = -2$ in a junction, $P_{R_d = A}$ when $u = 2$ is equal to $P_{R_d = Z}$ when $u = -2$. When $u < 0$, asymmetrical junctions are favored while $u > 0$ favors symmetry. Using Eqns 4 and

5 with a u range of −5 to 5 created trees that populated the P_f range from maximum asymmetry ('fishbone' trees) to perfect symmetry (WBE trees). For a given tree, we fixed u at a single value. When u was varied within a tree to produce both strongly symmetric and asymmetric junctions, the generated trees were unrealistic (Fig. S2).

As an illustration of the daughter selection process, consider the circled junction in Fig. 2 (left tree). This tree has 10 twigs total and $u = -2$ was selected at random from −5 to 5. First, $f^* = 3$ was selected from 2, 3 or 4 with equal probability. The f of the first junction (the trunk; with $R_m = 10$) was chosen between 2 and f^* with equal probability. Choosing $f = 3$, the rank of the smallest daughter, $R_{d,1}$, was selected next. Because $R_{d,1}$ is the smallest and all daughters must add up to 10, $R_{d,1}$ must be between 1 (A_1) and 3 (Z_1), as given by Eqn 2. With negative u, $R_{d,1} = 1$ will have the greatest probability ($P_{R_{d,1}} = 0.735$ from Eqn 4) and 3 will be very unlikely ($P_{R_{d,1}} = 0.082$). Suppose $R_{d,1} = 1$ is chosen. The second daughter, $R_{d,2}$ is the next smallest so it may range from 1 to 4, as given by Eqn 3. Again, the minimum, 1, is most likely to be chosen. Here, $R_{d,2} = 2$ was chosen. The final daughter has only one option, $R_{d,f} = 7$, resulting in a fairly asymmetrical junction. After creating this first junction, each daughter with $R_d > 1$ became a mother and junction selection continued, keeping $f^* = 3$ and $u = -2$. The right tree in Fig. 2 shows how $u = +2$ can create much more symmetrical junctions.

Branch diameters After assigning all ranks, branch diameters and lengths were determined. Diameters were defined using constant twig diameters and area preservation (i.e. $D_m^2 = \sum_{i=1}^{r} D_{d,i}^2$). With R defined as the total number of supported twigs, each with constant cross-sectional area, R is proportional to the cross-sectional area of the branch. As such, diameter, D, is a function of R and twig diameter, D_t:

$$D = D_t R^{0.5} \qquad \text{Eqn 6}$$

This property is illustrated by the trees in Fig. 2 where diameters increase with R.

Branch lengths Length determination is more complicated but the guiding principle is that lengths must coordinate with diameters to achieve a constant safety factor from whole-tree elastic buckling from branch weight. Here, we define a new pathlength, $L_{\uparrow}^*$, where the upward arrow indicates this length is from branch base (i.e. just above its lower junction) up to twig tip. This contrasts with the double arrow in $L_{\updownarrow}$ which indicates trunk to twig path. The asterisk in $L_{\uparrow}^*$ signifies the maximum pathlength (i.e. to the most distant twig).

Empirical data indicate that once a trunk or branch reaches a modest D, its longest supported path, $L_{\uparrow}^*$, tends to scale as $L_{\uparrow}^* \approx aD^{2/3}$ (Niklas, 1994; von Allmen *et al.*, 2012). The exponent of 2/3 is consistent with elastic similarity (i.e. constant deflection per length; McMahon & Kronauer, 1976). The critical height at elastic buckling, L_{crit}, is also predicted to follow 2/3 scaling with D: $L_{crit} = bD^{2/3}$, where b can be explicitly calculated from tree form and wood properties (Greenhill, 1881). The shared 2/3 exponent means the safety factor from buckling ($L_{crit}/L_{\uparrow}^*$) becomes constant at larger D. This ultimately constant safety factor, s, is equal to the ratio of the scaling multipliers: $s = b/a$. At smaller D, however, the $L_{\uparrow}^*$ by D scaling is steeper than 2/3. McMahon & Kronauer (1976) attribute this steeper exponent to a 'virtual length', l_o. If the tree is represented as an elastically similar doubly tapered beam, then l_o is the distance from the free end of the beam (i.e. the twig tip) to the point where the beam would taper to zero at its theoretical origin. McMahon & Kronauer (1976) show that $L_{\uparrow}^*$ by D scaling across all D can be fitted by an equation of the form:

$$L_{\uparrow}^* = aD^{2/3} - l_o \qquad \text{Eqn 7}$$

As D increases, the l_o term becomes comparatively negligible and the equation converges to $L_{\uparrow}^* = aD^{2/3}$ (see Fig. S3).

Branch lengths were assigned from a single version of Eqn 7 (Eqn 8) that was applied across all trees regardless of their branching topology. The multiplier, a, was defined as $a = b/s$, where $s = 4$ and b was calculated from a WBE tree ($b = 107.94\,\mathrm{m}^{1/3}$; see Mechanical stability section below). The value of l_o was derived from WBE trees (see Notes S2) and plugged into Eqn 7 to produce the $L_{\uparrow}^*$ by D equation for all modeled trees:

$$L_{\uparrow}^*(D) = \frac{b}{s} D^{2/3} - 0.794 \frac{b}{s} D_t^{2/3}. \qquad \text{Eqn 8}$$

Equation 8 gives maximum length distal to each branch segment and from this, individual branch lengths (i.e. between junctions) were determined. At a given junction, the mother branch will have a certain $L_{\uparrow}^*$ and its daughters will have respective $L_{\uparrow}^*$ values. Because larger diameters support longer paths, it will be true that the daughter with the largest diameter, D_d^*, will be part of the mother's longest path. Therefore, the segment length of the mother, l_m, is

$$l_m = L_{\uparrow}^*(D_m) - L_{\uparrow}^*(D_d^*). \qquad \text{Eqn 9}$$

Twigs, which do not support daughters, have lengths equal to their $L_{\uparrow}^*$:

$$l_t = L_{\uparrow}^*(D_t). \qquad \text{Eqn 10}$$

The use of Eqn 9 can be illustrated by the left tree in Fig. 2. The trunk ($R_m = 10$) supports a maximum path of $L_{\uparrow}^* = 0.58$ m (using model parameters in Eqn 8). Of its three daughters, only the largest daughter ($R_d^* = 7$) lies along this path. This daughter supports a maximum path of $L_{\uparrow}^* = 0.48$ m. Therefore, the length of the trunk segment must be the difference: $l_m = 0.10$ m.

Hydraulic conductance of model trees

The hydraulic conductance, K, for each model tree was calculated from the internal network of xylem conduits. The internal

anatomy is defined from the external anatomy following the recent WBE revision by Sperry *et al.* (2012). Briefly (see Notes S3 for details), hydraulic conductance of each stem segment is calculated from the diameter, number and length of functional xylem conduits (Savage *et al.*, 2010; Sperry *et al.*, 2012). Additional hydraulic resistances come from leaves, roots and conduit endwalls (Sperry *et al.*, 2012). Segment conductances were combined using rules of network analysis to calculate K.

Sperry *et al.* (2012) used the external branching parameters of WBE to study the effects of variable internal anatomy. Here, we did much the opposite, using Sperry *et al.*'s default internal parameters while studying the consequences of branching pattern and P_f on hydraulic conductance and the hydraulic exponent, q.

Volume of model trees

Tree volumes were calculated to determine their sensitivity to P_f and, hence, the sensitivity of the volume exponent, c. Total stem volume, V, was the summed volume of all cylindrical branch segments. The volume of roots and leaves was not computed but assumed to be proportional to stem volume. If tissue density is invariant, then V becomes a proxy for stem (and plant) mass for purposes of metabolic scaling predictions.

Mechanical stability of model trees

The effect of branching structure on mechanical stability was assessed for all model trees by comparing estimated critical heights at elastic buckling (L_{crit}) relative to estimated L_{crit} of WBE trees ($L_{crit,WBE}$). Typically, L_{crit} is estimated by folding all branches up to make a column and assuming that the tree mechanically behaves as this column (Niklas, 1994). Furthermore, this column is assumed to have straight sides. To represent the full spectrum of more realistic trees, we used the alternative method of Jaouen *et al.* (2007), which identifies the 'main stem' (i.e. the thickest trunk-to-twig path) as the tallest mechanical structure which must support itself and all attached branches. The Jaouen *et al.* method accounts for the important effects of branching architecture on vertical mass distribution and L_{crit}. The diameter, D, of the main stem may be described as a function of height, z, using

$$D = D_T\left(1 - \frac{z}{L^*_{\uparrow}}\right)^n \qquad \text{Eqn 11}$$

Likewise, the stem mass of all branches supported above z may be defined by

$$M = M_{tot}\left(1 - \frac{z}{L^*_{\uparrow}}\right)^m \qquad \text{Eqn 12}$$

where M_{tot} is the total tree stem mass. The exponents n and m approximate the distributions of support capacity (D) and support requirement (M) in the main stem. For each tree, these exponents were calculated from Eqns 11 and 12 by standardized major axis (SMA) regression of logged data using the SMATR package for R (http://bio.mq.edu.au/ecology/SMATR/; Warton *et al.*, 2006).

With some modifications to Jaouen *et al.*'s Eqn 1 (see Notes S4), we predicted L_{crit} using

$$L_{crit} = \frac{c_v^{2/3}(|m - 4n + 2|)^{2/3}}{4P_f^{1/3}}\left(\frac{E}{\rho_g}\right)^{1/3} D_T^{2/3} \qquad \text{Eqn 13}$$

Values for the ratio of E (Young's elastic modulus; N m^{-2}) and ρ_g (specific weight of supporting tissue; N m^{-3}) for wood are approximately constant (Niklas, 1994). The c_v (determined numerically in R) is the first positive root of the Bessel function of the first kind with parameter $v = (4n-1)/(m-4n+2)$ (Greenhill, 1881; Jaouen *et al.*, 2007). The value of b in Eqn 8 corresponds to all the terms in front of $D_T^{2/3}$ in Eqn 13 where m, n, c_v and P_f were from a WBE tree. When calculating L_{crit}, two requirements were imposed. (1) Values of n and m are only meaningful when the data are well fitted by Eqns 11 and 12. We removed trees where fits had $r^2 < 0.95$. (2) When $v < -1$, the c_v becomes somewhat erratic so these trees were also removed. Less than 7% of all modeled trees were removed for poor fits to Eqns 11–12 and only three trees in total were excluded for $v < -1$.

Light interception of model trees

The importance of light interception is implied in the WBE model through 'space-filling branching' but it has not been quantified (Duursma *et al.*, 2010). To estimate how P_f influenced light interception, we extended the model to three dimensions. For simplicity, we restricted 3D construction to trees where $f^* = 2$ was chosen. Determining spatial structure required specification of branching angles and rotations with respect to connecting stem segments. Each branch segment was assigned an axis that runs along its length. 'Branching angle' shall refer to the angle a daughter axis makes *away* from its mother's axis. 'Rotation' refers to the rotation *around* its mother's axis. We adopted a set of maximally simple rules to set these angles and applied them equally across modeled trees. Thus, we emphasize the general effects of P_f on light interception and not secondary influences of branching angle variation.

To our knowledge, the only work that comes close to a general branching angle theory for plants is Murray's (1927) volume minimization equations (see also Zhi *et al.*, 2001). However, these equations are inconsistent with area-preserving branching (two symmetric, area-preserving daughters are predicted to not diverge at all from their mother's axis). Nevertheless, Murray's (1927) Eqns 2–3 do produce realistic branch angle trends and so, despite their theoretical short-comings, we used them.

For rotation, daughters diverge from their mother's axis in opposite directions. Therefore, the daughters lie in the same plane. Accordingly, the mother also shares a plane with its sister branch. Each daughter plane was rotated 137.5° relative to its mother plane. The actual angle of rotation will depend on phyllotaxy and exactly which buds are released to form branches.

However, our model is not an ontogenetic one and 137.5°, the golden angle, is often observed and may minimize self-shading (Valladares & Brites, 2004).

As part of the 3D construction, we calculated crown area by projecting each tree from above and drawing a convex boundary linking the twig tips. Crown areas were used to estimate P_f from angiosperm crown scaling data of Olson *et al.* (2009; see 'Empirical path fractions', above). We also quantified tree shape as the aspect ratio (height/width). Height was actual height (instead of $L^*_{\updownarrow}$), which was similar for all trees with equivalent twig numbers. Crown width was obtained from the diameter of a circle with equivalent area to the crown area.

The 3D trees were subjected to a light interception model using the turbid medium analogy (Campbell & Norman, 1998). Following Sinoquet *et al.* (2001), the three-dimensional space occupied by each tree was discretized into voxels (i.e. 3D pixels) of side length l_{vox}. LAI of each voxel was calculated from the number of twig tips it contained and leaf area per twig (0.01 m^2). Interception by stems was ignored and we only modeled direct light with PPFD = 1500 μmol PAR $m^{-2}s^{-1}$. To address the effect of source angle, we specified zenith angles every 3° from horizontal to directly overhead. For each zenith angle, we averaged light interception from eight azimuth angles. For each source angle, voxels were delineated to form columns parallel to the light source. As such, the LAI of each column of voxels was calculated. Absorbed PAR (μmol s^{-1}) is

$$\mathrm{PAR}_{abs} = l_{vox}^2 \mathrm{PPFD} \sum_{i=1}^{N_c} [1 - \exp(-G_i LAI_i)] \qquad \text{Eqn 14}$$

(where N_c, the number of voxel columns; G, the ratio of projected and one-sided leaf area (Sinoquet *et al.*, 2001)). Leaves were considered spherically arranged, making $G = 1/2$ for all columns and independent of source angle (derived from Monteith & Unsworth, 1990).

Scaling predictions

Using K, V and D_T from the model, we tested how deviation from WBE branching affected the scaling exponents in: $K \propto D_T^q$; $V \propto D_T^{1/c}$; and $K \propto V^{cq}$. We identified three scaling scenarios (S_1, S_2 and S_3) for the relationship between P_f and tree size. Scenario S_1 was a constant P_f with increasing tree size. Size-invariant P_f is perhaps most comparable to WBE scaling as WBE trees always have $P_f = 1$. We selected six target P_f values from 0.4 to 1.0. We then modeled 10 000 trees at each of seven twig counts from 2^6 to 2^{12} twigs and isolated trees which had a P_f within 0.005 of each target. For trees with 2^5 twigs or fewer, $P_f = 0.4$ was not possible. The maximum twig number was limited by computation time.

Scenario S_2 modeled the observed decrease in P_f with size from our P_f measurements. In this scenario, we fit a log function to our inter-specific P_f vs twig number data. We used this function to choose a target P_f at each modeled size up to 2^9 twigs (near the maximum in our data) and selected individuals that matched each P_f target ± 0.005.

In scenario S_3, we used the P_f ontogeny estimated from Olson *et al.*'s (2009) angiosperm crown scaling data. The Olson *et al.* data covered a wider range of tree sizes. To accommodate this range, we built a limited set of 3D trees with up to 2^{18} twigs (D_T = 1024 mm). The subset of modeled trees that followed the crown scaling data showed a P_f-decreasing phase in small trees (as in our empirical measurements), followed by a P_f-increasing phase in larger trees (see Results). We defined the phase boundary at 2^{11} twigs and modeled the scaling exponents separately for each P_f phase: $2^6 - 2^{10}$ twigs (P_f decreasing) and $2^{12} - 2^{18}$ twigs (P_f increasing). For all scaling scenarios, we obtained q, c and cq from SMA regressions of logged data.

Results

Measured, modeled and estimated path fractions

The P_f range is bound by WBE trees at the maximum ($P_f = 1$) and 'fishbone' trees at the minimum. Among modeled trees, a high P_f corresponded to a broad crown (aspect ratio near one) while low-P_f trees had narrower crowns (larger aspect ratio; Fig. 1a,b). Among our 40 P_f measurements from real plants, P_f ranged from 0.357 to 0.930. No specimen met either the WBE prediction or the 'fishbone' prediction. There was a significant trend for P_f to decrease with increasing size (Fig. 3, characters and solid regression line). While these data included both whole individuals (black) and branches (white), regressions fitted to

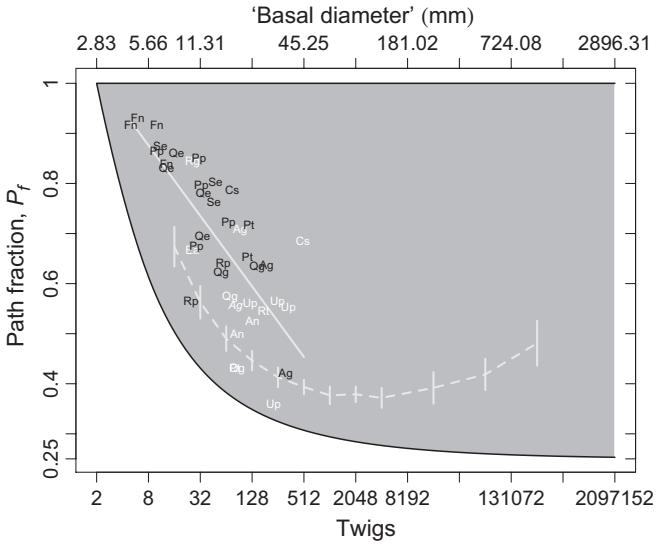

Fig. 3 Modeled range of possible P_f values (shaded) across a large range of twig numbers and basal diameters. Basal diameters assume a twig diameter of 2 mm and are only shown to give a sense of scale. Maximum P_f is 1.0 by definition and includes WBE trees. Minimum P_f uses a 'fishbone' structure with twigs attached alternately (i.e. $f = 2$) to a central axis (e.g. Fig. 1a, leftmost tree). Characters indicate empirical P_f values in 15 species (abbreviations and values in Table 2). Whole individuals are in black and branches are in white. The solid regression line through all empirical values ($P_f = -0.102 \log_e(\text{twigs}) + 1.088$) was used as the basis for scaling scenario S_2. The dashed line (mean ± SD) is based on crown area scaling from Olson *et al.* (2009) and was used for scenario S_3.

each were not significantly different. Parallel to the observed decline in empirical P_f, the model predicts that as trees add twigs, the minimum possible P_f (the 'fishbone' structure) rapidly decreases from 1 before asymptoting around 0.25 (Fig. 3, shaded area). It makes sense that the potential to deviate from WBE becomes greater with more twigs. More twigs equals more and larger junctions and, therefore, more and greater opportunities to be asymmetrical.

Analysis of the Olson *et al.* (2009) data indicated a two-phase P_f trajectory (Fig. 3, dashed line). The first phase, in smaller trees ($D_T < c.6$ cm), was a decline in P_f similar to what we measured. The second phase in larger trees showed a bottoming out of P_f followed by a gradual increase for $D_T > c.12$ cm.

P_f and whole-tree hydraulic conductance

The model was run to produce 10 000 trees at each of nine different twig counts (2^4–2^{12}). However, to illustrate the functional consequences of P_f, we only show 1024-twig trees as a representative. Similar trends were evident at all modeled tree sizes. Deviation from WBE structure (i.e. lower P_f) tended to increase K (Fig. 4a) with the 'fishbone' structure having the greatest conductance and the WBE structure having the lowest. A more than two-fold increase was observed across the P_f range in the 1024 twig example with all trees having the same basal diameter and height. As P_f decreased, K increased because the average transport distance from trunk to twig decreased. Shorter average transport distances translated into higher average trunk-to-twig conductances. For each tree size, the K vs P_f data were fit with power functions. All fits were very good ($r^2 > 0.98$). Some of the residual K variation was due to f^* with linear regressions of residuals vs f^* producing positive correlations with $r^2 = 0.30 \pm 0.09$ (mean $\pm$ SD). Hence, larger f^* tended to increase K at a given P_f. This is expected because greater f means branches become thicker (i.e. greater hydraulic conductivity) at a faster rate.

P_f and total stem volume

Reducing P_f caused V to decrease in a singularly linear fashion (Fig. 4b). Perfect linearity exists because of area-preservation and invariant twig diameters. As such, each $L_{\updownarrow}$ represents a 'tube' of tissue with constant volume per length, as in the pipe model (Shinozaki *et al.*, 1964). This relationship allowed us to define the volume fraction, V_f, as a corollary to P_f. The stem volume of each tree was standardized by the volume of a cylinder with equivalent height and basal diameter,

$$V_f = \frac{V}{\frac{\pi}{4} L^*_{\updownarrow} D_T^2} \qquad \text{Eqn 15}$$

For modeled trees, $V_f = P_f$. The volume of a WBE tree is that of the reference column (i.e. $V_f = 1$). Other structures have lower V_f due to volumes less than the reference column (i.e. profiles more akin to a frustum).

P_f and mechanical stability

The L_{crit} relative to the WBE tree was lowest near $P_f = 1$ (6.46% lower) and greatest near minimum P_f (30.97% greater; Fig. 4c). This P_f-dependent trend was due to the effects of m, n

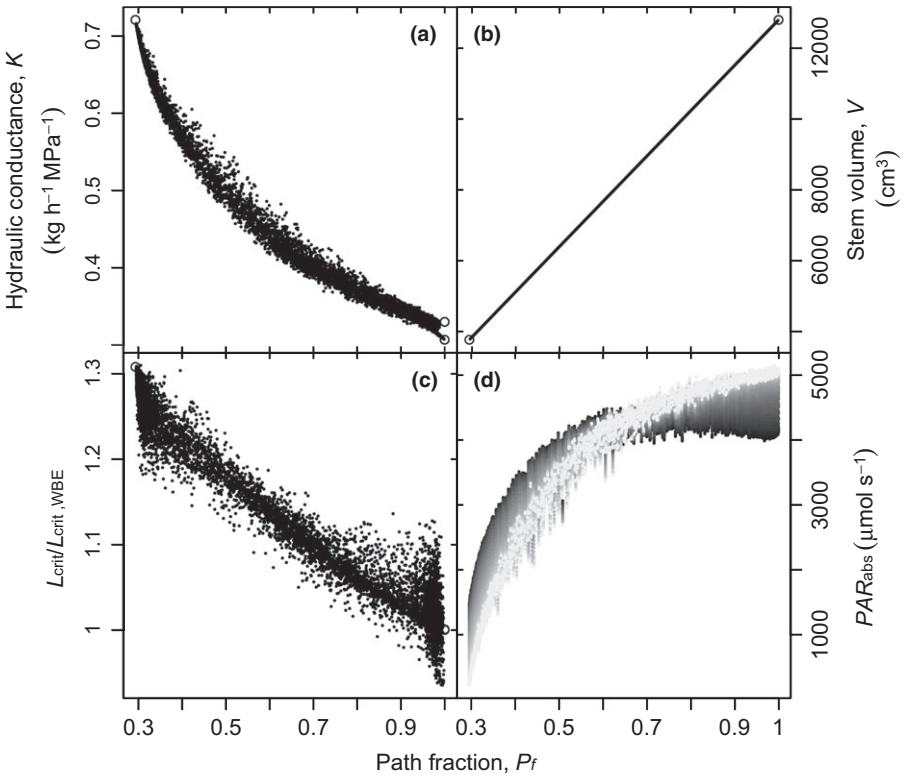

Fig. 4 Predicted tree function vs path fraction. Simulations are shown for trees with the same basal diameter, height and twig number (1024), but the same trends applied regardless of tree size. In (a)–(c), open circles represent the P_f extremes. (a) Tree hydraulic conductance decreased with P_f. The open circles at $P_f = 1$ correspond to $f^* = 4$ (upper) and $f^* = 2$ (lower). (b) Total stem volume increased in perfect linear proportion to P_f. (c) The critical height at elastic buckling, L_{crit}, relative to a WBE tree decreased with P_f. (d) Tree light absorption increased with P_f at all light source angles, but more strongly so as source angle shifted from horizontal (black) to vertical (shading to white).

and total stem mass. The mass distribution exponent, m, was fairly constant across the P_f range: 2.97 ± 0.10 (mean ± SD; $m = 1$ corresponds to a straight column, $m > 1$ to a tapered column). Near $P_f = 1$, m was quite variable, which is reflected in L_{crit} variability near $P_f = 1$ in Fig. 4c. Meanwhile, the main stem taper exponent, n, increased as P_f dropped (range = 0.93–1.23; $n = 0$ corresponds to a straight column). A larger n indicates stronger taper in the main stem and therefore less support tissue up high. This alone tends to reduce L_{crit}. However, a smaller P_f indicates there is less total mass that requires support and therefore greater L_{crit}.

Light absorption and P_f

Regarding light absorption, PAR_{abs}, we were limited to trees modeled in 3D (i.e. those with $f^* = 2$). Trees with the same number of twigs also have the same total leaf area. Therefore, for a given number of twigs, PAR_{abs} variations are solely due to different leaf arrangements. At a given zenith angle, PAR_{abs} increased with P_f such that 'fishbone' trees absorbed the fewest photons and WBE trees absorbed among the most (Fig. 4d). This P_f effect increased as the light angle was shifted from horizontal side-illumination to overhead.

Scaling and P_f

We modeled three scaling scenarios: S_1, P_f is constant through ontogeny of a particular species but can vary across species ($P_f = 0.4 - 1.0$; 2^6 to 2^{12} twigs); S_2, P_f decreases through ontogeny both within and across species, following the regression on our P_f data for small trees ($D_T < c.\,5$ cm; 2^6 to 2^9 twigs; Fig. 3, solid line); and S_3, P_f decreases in small trees (2^6–2^{10} twigs) and reaches a nadir before gradually increasing in larger trees (2^{12}–2^{18} twigs), as estimated from the Olson *et al.* (2009) data (Fig. 3, dashed line). In the three scenarios, the modeled data used for each scaling relationship (K by D_T^q, V by $D_T^{1/c}$ and K by V^{cq}) were well fitted by power functions ($r^2 > 0.99$).

The hydraulic exponent, q, was obtained from K by D_T^q relationships. In S_1, where P_f was constant with size, $P_f = 1$ predicted $q = 1.80$, which falls short of the original WBE prediction of $q = 2$ because of finite size effects and revisions to the internal anatomy (Savage *et al.*, 2010; Sperry *et al.*, 2012). As P_f decreased to 0.4, q increased to 1.85 (Fig. 5a); still shy of $q = 2$. In S_2, P_f decreased with size, which caused K to increase at a faster rate than for constant P_f. Therefore, q steepened to 2.04: very near the WBE requirement. Similarly, in S_3, as P_f decreased, hydraulic scaling steepened relative to constant P_f: $q = 1.96$. However, as P_f increased in larger trees, K increased more slowly and q decreased to 1.81.

Similar results existed for the volume exponent, c, in $V \propto D_T^{1/c}$. In S_1 (P_f constant through ontogeny), c was essentially unaffected by P_f: $c = 0.364 \pm 0.001$ (mean ± SD; Fig. 5b). All values were near but below the WBE prediction of $c = 3/8 = 0.375$. As shown by rearranging Eqn 15, $V = \frac{\pi}{4} V_f L_{\updownarrow}^* D_T^2$ and because $V_f = P_f$, an ontogenetically invariant P_f makes $V \propto L_{\updownarrow}^* D_T^2$, meaning the scaling exponents among trees or species with different but constant P_f will be identical. Over the modeled size range, $L_{\updownarrow}^*$ by D_T is not a perfect power function because it has yet to converge on $L_{\updownarrow}^* \propto D_T^{2/3}$ (Eqn 8). This fact, combined with a variable number of trees at each P_f-D_T combination, made $c < 0.375$ and created some variation in c. In scenario S_2 (P_f decreases through ontogeny), V increased at a slower rate relative to constant P_f, which lowered $1/c$ and increased c up to 0.41, exceeding the WBE prediction. When P_f decreased then increased (S_3), the decrease produced a steeper c (0.389) followed by a flatter c (0.355) as P_f increased in larger trees.

The metabolic exponent, cq, in $K \propto V^{cq}$, follows the q and c results. When P_f was constant through ontogeny, as in S_1, cq showed a meager increase from 0.655 at $P_f = 1$ to 0.671 at $P_f = 0.4$ (Fig. 5c), well below the WBE prediction of $cq = 0.75$ due to the same finite-size effects as above. However, when P_f decreased throughout growth of smaller trees (S_2), the larger q and c together exceeded the WBE prediction of 0.75: $cq = 0.843$. When P_f decreased and then increased with greater tree size (S_3), cq initially exceeded 0.75 (0.760), before decreasing below all other values: $cq = 0.642$ (see Fig. S4).

Discussion

In answer to our opening question, the results show that deviations from symmetrical WBE branching in real trees can be substantial and size dependent and these deviations have major effects on tree function and metabolic scaling. We used the path fraction, P_f, to quantify branching architecture in both real plants and modeled trees. We found that P_f in all of our real networks fell below the WBE ideal of $P_f = 1$. Furthermore, empirical P_f showed a biphasic ontogeny: first decreasing strongly with size before bottoming out at *c.* $D_T = 6 - 12$ cm and gradually increasing thereafter. Our model predicted significant effects of deviating from the symmetrical self-similarity of the WBE model. When twig number was held constant (meaning constant height, leaf area and basal diameter), deviating from WBE led to greater whole-tree hydraulic conductance (K), lower stem volume (V), greater critical buckling height (L_{crit}), and reduced total photon absorption (PAR_{abs}). When we 'grew' trees to different sizes we found that if P_f was held constant, deviations from WBE branching caused only a minor increase in the metabolic exponent, cq, owing to shifts in q. All cq values were below the original WBE prediction of 0.75. This was true even for WBE-branching trees because of finite size effects (Savage *et al.*, 2010) and hydraulic architecture modifications (Sperry *et al.*, 2012). If we assumed that P_f declined to a minimum before increasing with size, as observed interspecifically, the cq was size dependent. For small trees with decreasing P_f, cq could increase beyond 0.75 due to large increases in both c and q. But for larger trees with gradually increasing P_f, cq was much lower, falling below 0.65.

The 'U' shaped P_f trajectory estimated for real trees makes intuitive sense. Young trees may place a premium on height growth, which would be favored by P_f-decreasing crowns that become elongated and relatively narrow (Fig. 1b; Charles-Dominique *et al.*, 2012). High hydraulic conductance per tissue

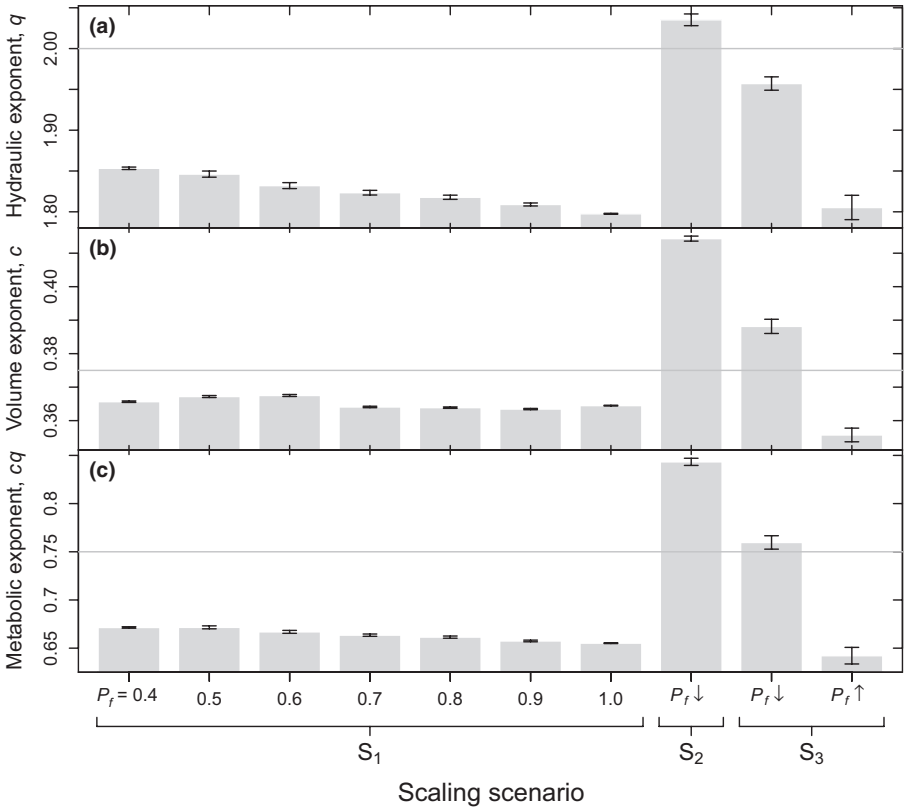

Fig. 5 Summary of SMA scaling exponents with 95% confidence intervals for the three P_f ontogenies we considered. In scenario S_1, path fractions were constant during growth. $P_f = 1.0$ includes WBE trees (constant f) as well as other trees that maintain perfect or nearly perfect junction symmetry but variable f. In S_2 and S_3, P_f was size dependent, either decreasing ($P_f\downarrow$) along the solid line in Fig. 3 (S_2; based on our data) or decreasing and then increasing ($P_f\uparrow$) according the dashed line in Fig. 3 (S_3; based on Olson *et al.* crown scaling). Horizontal lines indicate the original WBE predictions.

volume, and greater mechanical stability (or greater height per trunk diameter) of low-P_f crowns may also maximize height growth. As the tree reaches or exceeds the height of surrounding vegetation, broader high-P_f crowns would capitalize on greater light availability and fill canopy gaps.

For a given D_T and height, decreasing P_f was a strong predictor of increasing K. This result was somewhat surprising as P_f represents an entire branching structure with just mean and maximum pathlengths. However, the hydraulic conductance of a nontapering tube is inversely related to its length so it follows that K should increase as pathlengths are shortened (Fig. 4a). Indeed, individual trunk-to-twig hydraulic conductances within a tree were always negatively correlated with path length (not shown). In the model, the length-dependence of K is reduced but cannot be eliminated or reversed by observed xylem conduit taper or leaf resistance (Sperry *et al.*, 2012). Data on path conductance and actual path length are limited, but support the prediction of greater conductance for shorter trunk-to-leaf paths (Sperry & Pockman, 1993). Whole-path conductance to branches lower in the canopy can be equivalent to (Hubbard *et al.*, 2002; Yoshimura, 2011) or even lower than (Kupper *et al.*, 2005; Sellin & Kupper, 2005) branches higher up, but the pathlengths were not measured in these studies. However, it is possible that shorter paths could develop lower conductances if shading caused senescence or growth of narrower twigs (Protz *et al.*, 2000). Variation in twig properties within a canopy was not modeled, but could obscure the pathlength effect.

At the whole-tree level, the xylem architecture component of the model is known to yield realistic ranges of water use and K across different functional tree types (von Allmen *et al.*, 2012; Sperry *et al.*, 2012). Rigorous tests of the additional effects of branching await information on the ranges of P_f across major tree types. The P_f is a novel metric and there are no data on it outside of this paper. Although it is difficult to measure on large trees, in principle the model can be used to estimate it from the allometries of crown area and height vs trunk diameter. In real trees, the effects of variable branching structure are superimposed on effects of variable xylem anatomy. A virtue of the model is the ability to separate out the hydraulic contributions of these two networks.

The model showed that total stem volume decreased as P_f decreased (Fig. 4b). Trees with shorter transport distances on average require less construction tissue, even for the same height and basal diameter. Furthermore, V vs P_f was a perfect linear relationship, resulting in the volume fraction, V_f, being equal to the path fraction, P_f. The V_f is potentially much easier to estimate than P_f, which would facilitate its measurement in trees.

As P_f was decreased, the model also predicted that critical heights, L_{crit}, increased for a given D_T (Fig. 4c). The greater mechanical stability of conical low-P_f trees is an intuitive result because they carry more of their mass closer to the ground than round-crowned high-P_f trees. In the scenario we modeled, all trees of a given D_T were the same height. Therefore, the increase in L_{crit} resulted in greater safety from buckling in low-P_f trees. Alternatively, if trees grow towards the same safety from buckling, low-P_f trees should grow taller for a given D_T than high-P_f trees.

The latter prediction appears to be supported by the available data. Among temperate trees, evergreens (mostly conifers) have

been shown to grow taller with diameter than deciduous (mostly angiosperm) trees (Ducey, 2012). Although phenology was stressed in that study, our model suggests an alternative explanation: a tendency for large conifers to have a lower P_f may allow them to grow taller than angiosperms for the same trunk diameter. Lower P_f for large conifers is suggested by their tendencies to be taller (Ducey, 2012) and to have narrower crowns (see Fig. S1; Krajicek *et al.*, 1961; Vezina, 1962; Leech, 1984; Farr *et al.*, 1989) than similarly large-trunked angiosperms. Low P_f in large conifers would favor height growth per basal diameter by: increasing L_{crit}; decreasing volume investment; and increasing tree hydraulic conductance.

PAR_{abs} was also influenced by P_f (Fig. 4d). In WBE trees, symmetric branching means there is no distinct main stem and branches can spread large distances in all directions. As P_f is lowered, a distinct main stem starts to develop with branches extending from this stem (see Fig. 1a). This configuration limits the horizontal spread of branches, leading to more self-shading of leaves and less light absorption (Pearcy *et al.*, 2004a). Changing the light angle from vertical to horizontal reduced this disadvantage of low-P_f trees, but did not eliminate it. Lowering P_f should always limit the lateral spread of leaves, so using a different light model or alternative branching angles should not impact our general prediction.

Our results suggest how the local environment may select for optimal branching architecture. For three out of the four modeled tree properties (hydraulic conductance, volume, mechanical stability and light interception), low-P_f trees are at a competitive advantage as they can transport water more easily despite a smaller investment in tissue and have greater mechanical stability. However, these advantages come at the expense of reduced light absorption. Hypothetically, the diverse spectrum of tree forms in nature could result from optimizing this tradeoff for a diverse set

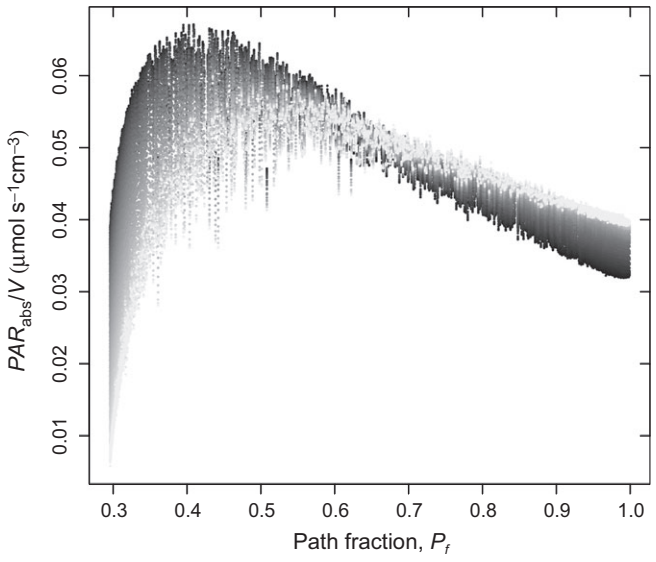

Fig. 6 Volume normalized light interception for the same trees shown in Fig. 4d. Shading corresponds to mean absorption at each zenith angle from horizontal (black) to directly overhead (white). The peaks observed at each zenith angle are suggestive of optimal architectures that maximize carbon gain per carbon spent.

of requirements, depending on life history and habitat (Horn, 1971). In general, selection for a given branching architecture will depend on the relative advantages of transporting water, growing fast, growing tall and gathering light. As already discussed, the optimal P_f of an angiosperm canopy tree may change through ontogeny, with decreasing P_f favoring early height growth followed by increasing P_f to favor canopy gap-filling (Horn, 1971). Alternatively, short shade-tolerant species adapted to the high humidity and low light of the understory are expected to always have a high P_f. Such species lack a prolonged height growth phase and need to avoid self-shading (Pearcy *et al.*, 2004b). The associated low hydraulic conductance would not be a liability for short stature and low evaporative demand. Conversely, high-P_f shrubs or treelets would also be expected in open habitats where competition for light is absent and height growth is less advantageous.

While it was beyond the scope of this study to fully quantify the tradeoffs of different architectures, the concept of a P_f optimum can be illustrated by normalizing PAR_{abs} by V. Fig. 6 shows broad peaks at midrange P_f for all light angles. Moving the light source from vertical to horizontal sharpened and elevated the peak and shifted it to lower P_f. Increasing the tree size had comparatively little effect on peak shape or position (not shown). As PAR_{abs} is closely tied to photosynthesis and V to mass, the results are suggestive of peaks in carbon gain per carbon spent. Photosynthesis will also depend on water supply to the leaves and its influence on stomatal conductance. As such, the higher K associated with lower P_f (Fig. 4a) would tend to further benefit the midrange-P_f trees relative to high-P_f trees.

Systematic changes in branching architecture with size, either through ontogeny or across species, have potentially major effects on metabolic scaling. With size-invariant P_f, changing P_f had fairly small effects on the hydraulic and metabolic exponents (q and cq). Much larger effects have been seen by changing the internal structure such as xylem conduit taper and sapwood area scaling (Sperry *et al.*, 2012). This result offers some support that the scaling of the WBE tree can be reasonably representative of non-WBE branching structures. This may explain why retaining the WBE structure resulted in generally good fits to sapflow data (von Allmen *et al.*, 2012). The result also shows agreement with Bentley *et al.* (2013) that junction asymmetry is not a predictor of whole-tree scaling. However, the P_f appears to change systematically with tree ontogeny, making scaling exponents size-dependent and allowing cq to reach or exceed the original WBE prediction of $cq = 3/4$ in small trees. Within the constraints of WBE architecture, the only other identified mechanism of $cq \geq 0.75$ in a finite individual is ontogenetically increasing the root-to-shoot hydraulic conductance ratio (Sperry *et al.*, 2012).

The model quantifies basic trade-offs between branching structure and major aspects of tree function. Narrow, elongated crowns are predicted to maximize vascular supply and mechanical stability, and minimize tissue investment. Broad, round crowns maximize light interception. No single shape is likely to be optimal across all habitats and tree sizes, and shape appears to shift though ontogeny. The model provides a framework for ultimately predicting optimal architectures. Although differences in

architecture exist across at least some functional tree types (e.g. angiosperm vs conifer), such variation needs to be expressed in terms of path fractions or the equivalent for a functional analysis. Our branching structure analysis adds another layer of complexity to the evolving theory of metabolic scaling in trees. The central, elegant predictions of the original WBE model for 3/4 scaling become fascinatingly complex when the variable structures of real plants are considered.

Acknowledgements

Mathematical interpretations were improved by discussions with Fred Adler. Peter Reich provided helpful input at various stages of the project. Jake Olsen and Erica von Allmen assisted with empirical measurements from Utah. We thank Will Driscoll for helping collect the ponderosa pine data. D.D.S. and J.S.S. were supported by NSF IBN-0743148. Funding from ATB Award 0742800 helped develop the initial ideas for this work.

References

von Allmen EI, Sperry JS, Smith DD, Savage VM, Reich PB, Enquist BJ, Bentley LP. 2012. A species' specific model of the hydraulic and metabolic allometry of trees II: testing predictions of water use and growth scaling in species with contrasting hydraulic traits. *Functional Ecology* **26**: 1066–1076.

Bentley LP, Stegen JC, Savage VM, Smith DD, von Allmen EI, Sperry JS, Reich PB, Enquist BJ. 2013. An empirical assessment of tree branching networks and implications for plant allometric scaling models. *Ecology Letters* **16**: 1069–1078.

Brodribb TJ. 2009. Xylem hydraulic physiology: the functional backbone of terrestrial plant productivity. *Plant Science* **177**: 245–251.

Campbell GS, Norman JN. 1998. *An introduction to environmental biosphysics, 2nd edn.* New York, NY, USA: Springer.

Charles-Dominique T, Edelin C, Brisson J, Bouchard A. 2012. Architectural strategies of *Rhamnus cathartica* (Rhamnaceae) in relation to canopy openness. *Botany* **90**: 976–989.

Ducey MJ. 2012. Evergreenness and wood density predict height-diameter scaling in trees of the northeastern United States. *Forest Ecology and Management* **279**: 21–26.

Duursma RA, Mäkelä A, Reid DEB, Jokela EJ, Porté AJ, Roberts SD. 2010. Self-shading affects allometric scaling in trees. *Functional Ecology* **24**: 723–730.

Farr WA, DeMars DJ, Dealy JE. 1989. Height and crown width related to diameter for open-grown western hemlock and Sitka spruce. *Canadian Journal of Forest Research* **19**: 1203–1207.

Greenhill AG. 1881. Determination of the greatest height consistent with stability that a vertical pole or mast can be made, and of the greatest height to which a tree of given proportions can grow. *Proceedings of the Cambridge Philosophical Society* **4**, 65–73.

Horn HS. 1971. *The adaptive geometry of trees.* Princeton, NJ, USA, Princeton University Press.

Horn HS. 2000. Twigs, trees and the dynamics of carbon in the landscape. In: Brown JH, West GB, eds. *Scaling in biology.* Oxford, UK: Oxford University Press, 199–220.

Hubbard RM, Bond BJ, Senock RS, Ryan MG. 2002. Effects of branch height on leaf gas exchange, branch hydraulic conductance and branch sap flux in open-grown ponderosa pine. *Tree Physiology* **22**: 575–581.

Jaouen G, Alméras T, Coutand C, Fournier M. 2007. How to determine sapling buckling risk with only a few measurements. *American Journal of Botany* **94**: 1583–1593.

Katifori E, Magnasco MO. 2012. Quantifying loopy network architectures. *PLoS ONE* **7**: 1–14.

Krajicek JE, Brinkman KA, Gingrich SF. 1961. Crown competition a measure of density. *Forest Science* **7**: 35–42.

Kupper P, Sellin A, Tenhunen J, Schmidt M, Rahi M. 2005. Effects of branch position on water relations and gas exchange of European larch trees in an alpine community. *Trees* **20**: 265–272.

Leech JW. 1984. Estimating crown width from diameter at breast height for open-grown radiata pine trees in South Australia. *Australian Forest Research* **14**: 333–337.

McMahon TA, Kronauer RE. 1976. Tree structures: deducing the principle of mechanical design. *Journal of Theoretical Biology* **59**: 443–466.

Monteith JL, Unsworth MH. 1990. *Principles of environmental physics, 2nd edn.* London, UK: Edward Arnold.

Murray CD. 1927. A relationship between circumference and weight in trees and its bearing on branching angles. *The Journal of General Physiology* **10**: 725–729.

Niklas KJ. 1994. The allometry of safety-factors for plant height. *American Journal of Botany* **81**: 345–351.

Niklas KJ, Enquist BJ. 2001. Invariant scaling relationships for inter-specific plant biomass production rates and body size. *Proceedings of the National Academy of Sciences, USA* **98**: 2922–2927.

Olson ME, Aguirre-Hernández R, Rosell JA. 2009. Universal foliage-stem scaling across environments and species in dicot trees: plasticity, biomechanics and Corner's Rules. *Ecology Letters* **12**: 210–219.

Pearcy RW, Muraoka H, Valladares F. 2004a. Crown architecture in sun and shade environments: assessing function and trade-offs with a three-dimensional simulation model. *New Phytologist* **166**: 791–800.

Pearcy RW, Valladares F, Wright SJ, de Paulis EL. 2004b. A functional analysis of the crown architecture of tropical forest *Psychotria* species: do species vary in light capture efficiency and consequently in carbon gain and growth? *Oecologia* **139**: 163–177.

Price CA, Enquist BJ, Savage VM. 2007. A general model for allometric covariation in botanical form and function. *Proceedings of the National Academy of Sciences, USA* **104**: 13204–13209.

Protz CG, Silins U, Lieffers VJ. 2000. Reduction in branch sapwood hydraulic permeability as a factor limiting survival of lower branches of lodgepole pine. *Canadian Journal of Forest Research* **30**: 1088–1095.

R Core Team. 2013. *R: a Language and environment for statistical computing.* Vienna, Austria: R Foundation for Statistical Computing. URL http://www.R-project.org/.

Savage VM, Bentley LP, Enquist BJ, Sperry JS, Smith DD, Reich PB, von Allmen EI. 2010. Hydraulic trade-offs and space filling enable better predictions of vascular structure and function in plants. *Proceedings of the National Academy of Sciences, USA* **107**: 22722–22727.

Sellin A, Kupper P. 2005. Variation in leaf conductance of silver birch: effects of irradiance, vapour pressure deficit, leaf water status and position within a crown. *Forest Ecology and Management* **206**: 153–166.

Shinozaki K, Yoda K, Hozumi K, Kira T. 1964. A quantitative analysis of plant form–the Pipe Model Theory: I. Basic analysis. *Japanese Journal of Ecology* **14**: 97–105.

Sinoquet H, Le Roux X, Adam B, Ameglio T, Daudet FA. 2001. RATP: a model for simulating the spatial distribution of radiation absorption, transpiration and photosynthesis within canopies: application to an isolated crown. *Plant, Cell & Environment* **24**: 395–406.

Sperry JS, Pockman WT. 1993. Limitation of transpiration by hydraulic conductance and xylem cavitation in Betula occidentalis. *Plant, Cell & Environment* **16**: 279–287.

Sperry JS, Smith DD, Savage VM, Enquist BJ, McCulloh KA, Reich PB, Bentley LP, von Allmen EI. 2012. A species' specific model of the hydraulic and metabolic allometry of trees I: model description, predictions across functional types, and implications for inter-specific scaling. *Functional Ecology* **26**: 1054–1065.

Valladares F, Brites D. 2004. Leaf phyllotaxis: does it really affect light capture? *Plant Ecology* **174**: 11–17.

Vezina PE. 1962. Crown width-DBH relationships for open-grown balsam fir and white spruce in Quebec. *Forestry Chronicle* **38**: 463–473.

Warton DI, Wright IJ, Falster DS, Westoby M. 2006. Bivariate linefitting methods for allometry. *Biological Reviews* **81**: 259–291.

West GB, Brown JH, Enquist BJ. 1997. A general model for the origin of allometric scaling laws in biology. *Science* **276**, 122–126.

West GB, Brown JH, Enquist BJ. 1999. A general model for the structure and allometry of plant vascular systems. *Nature* **400**: 664–667.

Yoshimura K. 2011. Hydraulic function contributes to the variation in shoot morphology within the crown in *Quercus crispula*. *Tree Physiology* **31**: 774–781.

Zhi W, Ming Z, Qi-Xing Y. 2001. Modeling of branching structures in plants. *Journal of Theoretical Biology* **209**, 383–394.

Supporting Information

Additional supporting information may be found in the online version of this article.

Fig. S1. Crown area vs diameter scaling showing data from angiosperms, conifers and modeled trees.

Fig. S2. Sample trees excluded from the model.

Fig. S3. Relationships between the three pathlength by diameter curves: critical; elastically-similar; and actual.

Fig. S4. K vs V scaling for model trees which follow Olson *et al.* (2009) crown scaling.

Notes S1. Plants used for empirical P_f: selection criteria and sources.

Notes S2. Derivation of Eqn 8 (pathlength).

Notes S3. Description of the xylem anatomy model.

Notes S4. Derivation of Eqn 13 (critical pathlength).

Please note: Wiley Blackwell are not responsible for the content or functionality of any supporting information supplied by the authors. Any queries (other than missing material) should be directed to the *New Phytologist* Central Office.